Journal of Hydrology 566 (2018) 73–88

Contents lists available at ScienceDirect

Journal of Hydrology

journal homepage: www.elsevier.com/locate/jhydrol

Research papers

A local-regional scaling-invariant Bayesian GEV model for estimating rainfall IDF curves in a future climate

Carlos H.R. Lima[a], Hyun-Han Kwon[b,*], Yong-Tak Kim[b]

[a] Dep. of Civil and Environmental Engineering, University of Brasilia, Brazil
[b] Dep. of Civil Engineering, Chonbuk National University, South Korea

ARTICLE INFO

This manuscript was handled by Marco Borga, Editor-in-Chief, with the assistance of Francesco Marra, Associate Editor

Keywords:
Rainfall
Intensity-Duration-Frequency curves
Bayesian model
Regional estimates
Climate change

ABSTRACT

Future changes in rainfall patterns induced by climate changes will affect society and ecosystems, and quantifying these changes is of utmost importance for the management of hydroclimate risk. In particular, the estimation of intensity-duration-frequency (IDF) curves for rainfall data is a routine procedure in urban hydrology and hydraulic studies and should be revisited to reflect future changes in rainfall variability. In this work, we propose a novel methodology based on the scaling-invariant property of rainfall duration versus intensity to estimate parameters of a generalized extreme value (GEV) distribution at sub-daily scales. A Bayesian inference framework is developed so that uncertainties are reduced and can be easily propagated to IDF curves. The proposed model can be employed to: (i) improve local (at-site) GEV estimates for sites with limited rainfall records; (ii) estimate GEV parameters at sub-daily scales and construct IDF curves for sites where only daily rainfall records are available (partially gauged sites); (iii) construct regional IDF curves for homogeneous hydrologic regions; and (iv) update local and regional IDF curves from simulations of future daily rainfall. The model is tested using historical rainfall data from 18 gauges located in the Han River Watershed in South Korea, and projected climate change scenarios RCP 6 and RCP 8.5 from the Met Office Hadley Centre HadGEM2-AO model. When considering historical data, the results show that the model satisfactorily estimate IDF curves for both gauged and partially gauged sites. In future scenarios, the model reveals a substantial increase in rainfall events of rare intensity (large return periods), mostly due to changes in the rainfall variability rather than changes in the average rainfall. Particularly, for a 100-year return period event, we expect an increase of about 23% in scenario RCP 6 and about 30% under scenario RCP 8.5 when projected using regional IDF curves. To the best of our knowledge, this is the first statistical approach in the literature to assess future changes in regional IDF curves, which in our opinion is more suitable than evaluating local estimates only.

1. Introduction

Statistics associated with extreme rainfalls play a major role in the design of hydraulic structures and hydrologic studies. In particular, the estimation of Intensity-Duration-Frequency (IDF) curves has primarily focused on analyzing historical rainfall records and estimating the intensity of an extreme rainfall event associated with a given rainfall duration and exceedance probability (or return period). Classical methods involve the fit of a probability distribution based on local data from rainfall gauges (e.g., Chow et al., 1988; Singh, 1992). In urban design, for instance, one is often interested in obtaining IDF curves at sub-daily time scales (1–24 h durations) for projects of macro drainage systems, which therefore requires rainfall records observed at least at the hourly scale.

The requirement of hourly rainfall records is possibly the first difficulty that arises when estimating IDF curves, since most rainfall surface measures around the globe still rely on traditional rainfall gauges, which are designed to record daily rainfall. To address this problem, some studies have adopted different disaggregation schemes (e.g., Koutsoyiannis, 1994; Sivakumar et al., 2001; Gyasi-Agyei, 2005; Segond et al., 2006) to simulate rainfall at shorter durations, while others have explored the scale-invariant assumption of rainfall intensity and duration (e.g., Nguyen et al., 1998; Koutsoyiannis et al., 1998a; Menabde et al., 1999; Muller et al., 2008) to show that local distribution estimates obtained for sites with sub-daily records (i.e. gauged sites) can be used to estimate parameters at sites where only daily rainfall is observed, hereafter referred as partially gauged sites, as denoted in Nguyen et al. (1998).

* Corresponding author.
E-mail addresses: chrlima@unb.br (C.H.R. Lima), hkwon@jbnu.ac.kr (H.-H. Kwon), dydxkr@jbnu.ac.kr (Y.-T. Kim).

https://doi.org/10.1016/j.jhydrol.2018.08.075
Received 5 July 2018; Received in revised form 27 August 2018; Accepted 29 August 2018
Available online 01 September 2018
0022-1694/ © 2018 Elsevier B.V. All rights reserved.

Another complication appears due to the limited extension of rainfall records, even for gauged sites, where rainfall data at the desired temporal scales are still available. Since one is interested in extremes of rainfall, the Generalized Extreme Value (GEV) distribution is often adopted (e.g., Nguyen et al., 1998; Muller et al., 2008) due to its asymptotic properties in series of annual maximum data (for more details, see Coles, 2001). However, estimating IDF curves becomes very complicated for sites with limited or absence of rainfall records. It is well known that GEV estimates, particularly for the shape parameter, can be unreliable for limited data records (e.g., Martins and Stedinger, 2000). As an alternative, one can employ regional estimates of parameters and determine regional IDF curves that can be used for ungauged sites or even replace at-site (i.e. local) IDF curves (Nguyen et al., 1998; Yu et al., 2004; Ghanmi et al., 2016; Blanchet et al., 2016). In constructing regional IDF curves, one usually needs to estimate local parameters for a given set of gauged sites and assumes that those parameters vary smoothly across the region, applying then some spatial interpolation method (e.g. kriging).

Besides the difficulties involving limited rainfall records and unavailable data at the desired temporal scales, one still tends to assume that local and regional IDF curves are stationary, i.e., the statistics of rainfall extremes are assumed to be constant over time. However, in a changing climate, it is expected that the rising temperature will affect rainfall extremes (e.g., Berg and Hall, 2015; Zhang and Villarini, 2017), and the stationarity assumption may not hold anymore. Studies aiming to quantify the impact of climate changes on IDF curves routinely rely on future rainfall simulations obtained from General Circulation Models (GCMs) or Regional Climate Models (RCMs), which require the use of a statistical or dynamical model to downscale the future simulation of rainfall to the temporal and spatial scales needed, since often rainfall products from GCMs are for large regions and at daily scale. Different examples of applications and methodologies to update IDF curves in a changing climate are presented and discussed in some recent works (Lima et al., 2016; Li et al., 2017; Ragno et al., 2018; Hosseinzadehtalaei et al., 2018).

We observe, however, that the focus has been primarily on assessing future changes in local IDF curves based on downscaling areal rainfall projections from GCMs, which might introduce severe bias in the estimates due to the inherent difficulty of GCMs to reproduce the correct spatial variability of rainfall. Future changes in ungauged sites or regional IDF curves have attracted less attention and deserve more studies. In this paper, we focus primarily on providing regional IDF curves based on the scaling property of rainfall as described in other studies (Menabde et al., 1999; Yu et al., 2004; Blanchet et al., 2016). We estimate the scaling-invariant parameters within a Bayesian framework, which allows us to derive regional estimates of the scaling coefficients and, therefore, regional IDF curves for the present and future climate given historical rainfall data and GCM projections of daily rainfall at any specified spatial scale. The proposed framework also provides better estimates of local IDF parameters, since it includes more information during the inference process, as well as supports a better strategy to deal with parameter uncertainties. Finally, the scaling parameters derived from the model can also be used to build IDF curves for partially gauged sites, where only daily rainfall is available. We test the proposed model using historical rainfall data from 18 gauges located in South Korea and projected climate change scenarios RCP 6 and RCP 8.5 provided by the Met Office Hadley Centre HadGEM2-AO model.

The rest of this study is organized as follows. The study area, rainfall data, and climate change scenario simulations are presented in Section 2. The methodology describing the proposed model is introduced in Section 3. In Section 4 we present the results, including the estimation of local and regional IDF curves for the historical and future periods. Finally, in Section 5, we offer a discussion and a summary of this study.

2. Study area, rainfall data, and scenario simulations

2.1. Han-River watershed and rainfall data

The Han-River Watershed was selected as a case study area to explore changes in design rainfall because the river serves as a primary water supply for over 12 million people in the Seoul area. The Han-River watershed is one of the largest watersheds in South Korea, having an area of about 35,800 km^2 and a total length of approximately 490 km long, which is the fourth longest river in the Korean peninsula. The annual precipitation and the annual average runoff are about 1208 mm and 613 m^3/s, respectively. For estimation of IDF curves, annual maximum series of rainfall intensity at hourly scale are routinely utilized. In this perspective, the 44 year, spanning the period 1973–2016, hourly precipitation data of 18 gauging stations for the entire Han-River watershed were compiled from the Automatic Synoptic Observation System (ASOS), operated by the Korean Meteorological Administration (KMA). The annual maximum series corresponding to different durations are then obtained from the hourly rainfall series for subsequent frequency analysis utilizing the sliding maxima approach (or *S*-maxima, as discussed in van Montfort (1990) and Papalexiou et al. (2016)). Fig. 1 shows the location of the Han-River watershed in Korea along with the rainfall gauges used in this work. Some basic summary statistics of the hourly rainfall data, including an L-Moment ratio diagram for different durations, are provided as Supplementary material.

2.2. Scenario simulation

The National Institute of Meteorological Research (NIMR) under KMA has adopted an Atmosphere-Ocean coupled General Circulation Model (HadGEM2-AO) for jointly participating in the Coupled Model Intercomparison Project phase 5 (CMIP5) with Met Office Hadley Centre. The HadGEM2-AO has been utilized to explore climate responses of Representative Concentration Pathways (RCPs) and offer future climate change scenarios over South Korea (Baek et al., 2013). More specifically, several GCM-based control experiments were carried out to simulate transient changes in climate and to further investigate the effects of the greenhouse gas concentrations on both current climate for the reference period (i.e., 1950–2005) and future climate for the future period (i.e., 2006–2100). In the experiments, the four RCP scenarios corresponding to different greenhouse gas integrations (i.e., RCPs 2.6, 4.5, 6.0, and 8.5) for the HadGEM2-AO were explored for the 95-year future climate simulations from 2006 to 2100. The atmosphere and ocean spatial horizontal and vertical resolutions of the HadGEM2-AO GCM are approximately N96 (135 km) L38 for the atmosphere system and 1 degree L40 for the ocean system.

Conversely, it has been well documented that there is a limitation of the GCM to represent local scale climate system due to a substantially coarser spatial resolution than half a degree. Regional climate models (RCMs) are commonly employed to dynamically downscale the large scale climate patterns to those of the regional (or local) scale under climate change for a particular sub-region, forced by surface and lateral boundary conditions derived from GCMs. In this context, a HadGEM3-RA RCM, which has spatial resolution of 12.5 km (0.11 degree), coupled with the GCM HadGEM2-AO has been adopted by KMA for climate change experiments. For additional details, the reader can refer to other articles that address the atmospheric physics and dynamics of the model (Davies et al., 2005; Ringer et al., 2006). Among the four RCP scenarios, we selected the most extreme RCP 6.0 and 8.5 for exploring future changes in the annual maximum daily rainfall for the Han-River watershed.

It has also been reported that climate models tend to underestimate daily rainfall amounts; conversely, the probability of rainfall

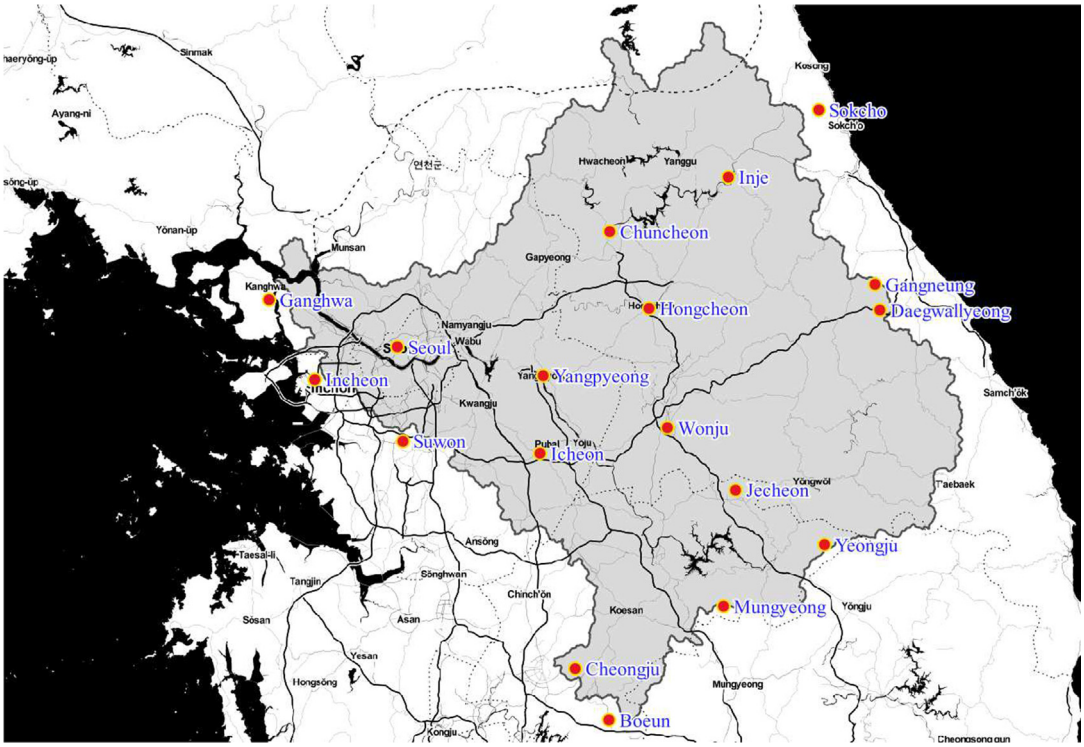

Fig. 1. Location of the Han River watershed in Korea, along with the 18 rainfall gauges (red dots) used in this work. (For interpretation of the references to colour in this figure caption, the reader is referred to the web version of this article.)

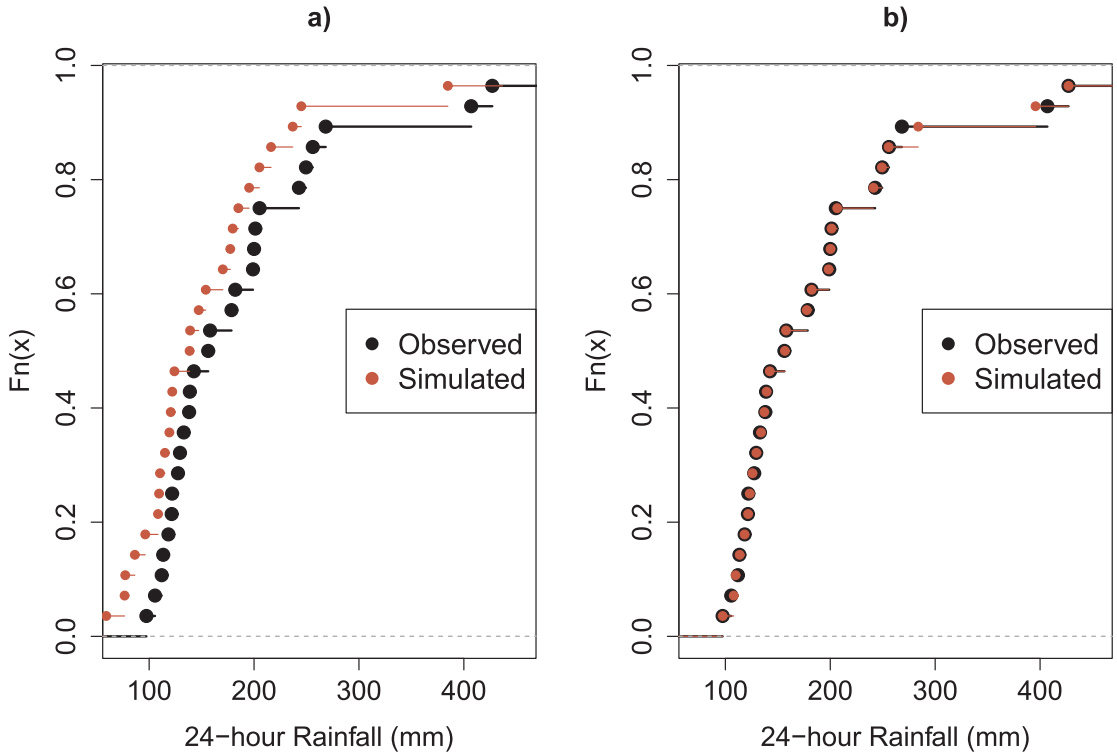

Fig. 2. Empirical cumulative distribution function for the 24-h annual maximum rainfall of observed (black dots) and simulated data (red dots) before (panel (a)) and after (panel (b)) the application of bias correction. The reference period is 1979–2005, and the benchmark station is Daegwallyeong. (For interpretation of the references to colour in this figure caption, the reader is referred to the web version of this article.)

occurrence is typically overestimated. To be more specific, light rain is overestimated, whereas moderate and extreme rainfalls are more or less underestimated over the Korean Peninsula (Lima et al., 2016; So et al., 2017). For this reason, this study adopted a smoothing spline-based bias correction approach (Gudmundsson et al., 2012) to correct the quantiles of simulated daily rainfall series for both the reference and the future periods. For each of the 18 gauging stations analyzed in this work, we extracted the daily rainfall simulated at the grid point

containing the gauging station of interest. For the purpose of comparison, the empirical cumulative function of observed and simulated rainfall before and after bias correction is illustrated in Fig. 2 for one rainfall station. The bias correction procedure was repeated for the remaining 17 stations.

3. Model

For a given rainfall gauge, we assume that the rainfall intensity y associated with a duration d can be written as (Koutsoyiannis et al., 1998b):

$$y(d, T_R) = \frac{a(T_R)}{(d+\theta)^H}, \tag{1}$$

where T_r is the return period, $a(\cdot)$ a function of T_r, and $0 < H \leqslant 1$ and $\theta \geqslant 0$ are non-negative coefficients. More general expressions for the denominator in (1) are discussed in Grimaldi et al. (2011).

Blanchet et al. (2016) linked the IDF curves at two different durations d and d_0 through the relation:

$$y(d, T_R) = y(d_0, T_R)\cdot\left(\frac{d+\theta}{d_0+\theta}\right)^{-H}. \tag{2}$$

Following the relations discussed in Blanchet et al. (2016), we can assume the hypothesis of scaling and then connect the qth moment at two different durations:

$$E[Y_d^q] = \left(\frac{d+\theta}{d_0+\theta}\right)^{-Hq} E[Y_{d_0}^q] \tag{3}$$

where Y denotes the random variable associated with the rainfall intensity and q is the moment order at durations d and d_0.

If we further assume a GEV scaling model, then for any duration d, it is possible to show that the rainfall intensity Y_d follows a GEV distribution with location (μ), scale (σ) and shape (ξ) parameters given by (Nguyen et al., 1998; Blanchet et al., 2016):

$$\mu_d = \mu_{d_0}\cdot\left(\frac{d+\theta}{d_0+\theta}\right)^{-H} \tag{4}$$

$$\sigma_d = \sigma_{d_0}\cdot\left(\frac{d+\theta}{d_0+\theta}\right)^{-H} \tag{5}$$

$$\xi_d = \xi_{d_0}. \tag{6}$$

Note that there is no scaling in the shape parameter, and in the log-log scale, the relations for μ and σ become:

$$\log(\mu_d) = \log(\mu_{d_0}) - H\cdot\log\left(\frac{d+\theta}{d_0+\theta}\right) \tag{7}$$

$$\log(\sigma_d) = \log(\sigma_{d_0}) - H\cdot\log\left(\frac{d+\theta}{d_0+\theta}\right). \tag{8}$$

For urban rainfall design, one is often interested in the rainfall intensity at sub-daily durations, whereas rainfall observations are available at daily scale. Hence, although the choices of d and d_0 are arbitrary, it is interesting to assume $d_0 = d_{24} = 24$ h, and the scaling could be used to obtain the rainfall intensity parameters μ and σ at shorter scales (e.g., Blanchet et al., 2016). Moreover, the appropriate use of the scaling relations assume that the sampling frequency is the same across all durations, which might not be the case for daily rainfall records. To address this issue, one can use the Hershfield factor (e.g., Papalexiou et al., 2016; Blanchet et al., 2016) to obtain series of annual maximum rainfall of 24 h duration (S-maxima series) from series of annual maximum daily rainfall (F-maxima series).

3.1. The Bayesian approach

Bayesian inference has been adopted in a wide range of hydrology studies, and it is beyond the scope of this paper to explore this growing body of literature. We point the reader to Gaume et al. (2010), Haddad et al. (2012), Kwon et al. (2008), Liang et al. (2011), Lima and Lall (2010), Renard (2011), Renard et al. (2006), Viglione et al. (2013) and the references therein for a few examples of Bayesian inference in hydrology, including estimation of IDF curves (de Vyver, 2015, 2018; Lima et al., 2016; Mélèse et al., 2018; Ragno et al., 2018). Here in this work, the main purpose to adopt a Bayesian inference for the d-duration rainfall modeling is to offer a framework to estimate regional parameters along with their uncertainties that can be used to build IDF curves for the present and future climate.

We assume then, for a given rainfall gauge, that the annual maximum rainfall intensity Y_d for duration d, $d = 1, 2, \ldots, 24$ h, follows the GEV distribution:

$$Y_d \sim GEV(\mu_d, \sigma_d, \xi_d), \tag{9}$$

which in our context has cumulative distribution function defined as:

$$F(x;\mu, \sigma, \xi) = \exp\left(-\left(1+\xi\frac{x-\mu}{\sigma}\right)^{-\frac{1}{\xi}}\right), \tag{10}$$

so that $\mu + \sigma/\xi \leqslant x < \infty$ for $\xi > 0$ and $-\infty < x \leqslant \mu + \sigma/\xi$ for $\xi < 0$.

Under the Bayesian framework, we need to set prior distributions for the GEV parameters that should reflect some knowledge we have about them, if any. In this case, the scaling theory as displayed in Eqs. (6), (7), and (8), provides us with the necessary insight to construct prior distributions that express our knowledge about the relations that exist between the moments of the GEV distribution at different durations. Hence, we assume as prior distributions for μ, σ, and ξ:

$$\log(\mu_d) \sim N\left(\alpha - H\cdot\log\left(\frac{d+\theta}{d_{24}+\theta}\right),\ \tau_\mu^2\right) \tag{11}$$

$$\log(\sigma_d) \sim N\left(\beta - H\cdot\log\left(\frac{d+\theta}{d_{24}+\theta}\right),\ \tau_\sigma^2\right) \tag{12}$$

$$\xi_d \sim N(\bar{\xi},\ \tau_\xi^2), \tag{13}$$

where $N(\cdot,\cdot)$ denotes the normal distribution with respective mean and variance, α and β are, respectively, the GEV location ($\log(\mu_{d_{24}})$) and scale ($\log(\sigma_{d_{24}})$) parameters associated with the rainfall duration $d_{24} = 24$ h; H and θ are the scaling coefficients; $\bar{\xi}$ is an average shape parameter across the different durations; and τ_μ^2, τ_σ^2 and τ_ξ^2 represent the variance associated with the respective scaling processes.

As for hyperprior distributions, we assume independent and a mixture of weakly and noninformative distributions, taking into account our vague knowledge about the parameters:

$$\alpha \sim N(0, 10^6) \tag{14}$$

$$\beta \sim N(0, 10^6) \tag{15}$$

$$H \sim B(1, 1, 0, 1) \tag{16}$$

$$\theta \sim U(0, 10) \tag{17}$$

$$\bar{\xi} \sim B(9, 6, -0.5, 0.5) \tag{18}$$

$$\tau_\mu^2 \sim Inv{-}Gamma(0.01, 0.01) \tag{19}$$

$$\tau_\sigma^2 \sim Inv{-}Gamma(0.01, 0.01) \tag{20}$$

$$\tau_\xi^2 \sim Inv{-}Gamma(0.01, 0.01), \tag{21}$$

where $U(\cdot,\cdot)$ denotes the uniform distribution and associated lower and upper intervals, $B(\cdot,\cdot,a,b)$ is the beta distribution with lower and upper bounds a and b, respectively, and $Inv{-}Gamma(\cdot,\cdot)$ is the inverse gamma distribution with shape and scale parameters.

The priors for α and β are near-flat and similar to those used in Coles (2001) and de Vyver (2015, 2018), except that here a larger variance is

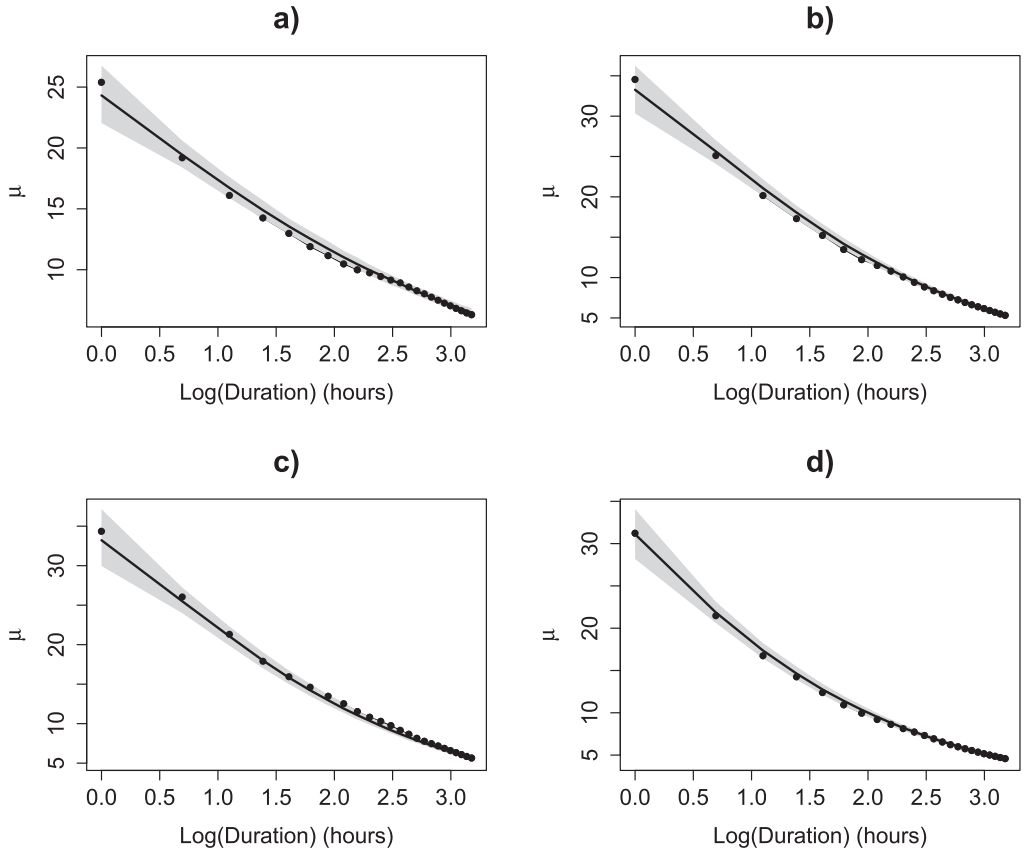

Fig. 3. Scaling of GEV location parameter μ using ordinary GEV (black dots) and the proposed local Bayesian model (black line) along with the 95% credible interval (shaded region) for benchmark gauges: (a) Daegwallyeong; (b) Suwon; (c) Yangpyeong; and (d) Boeun.

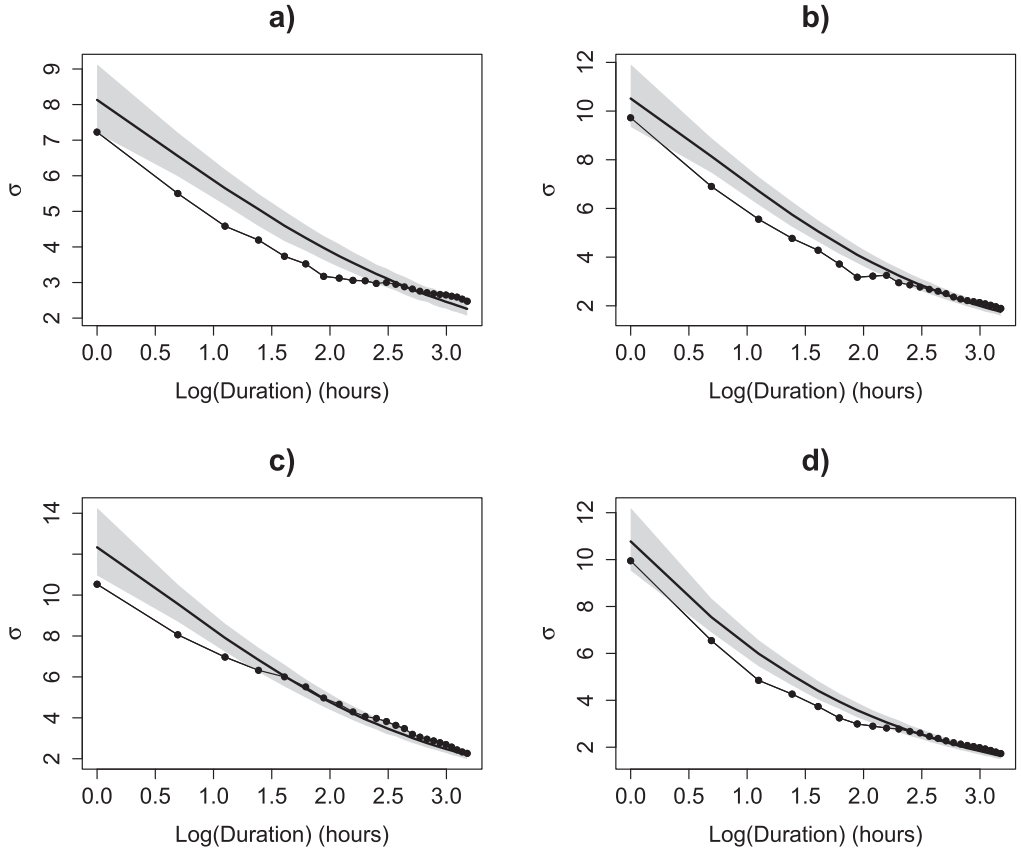

Fig. 4. As in Fig. 3, but for the GEV scale parameter σ.

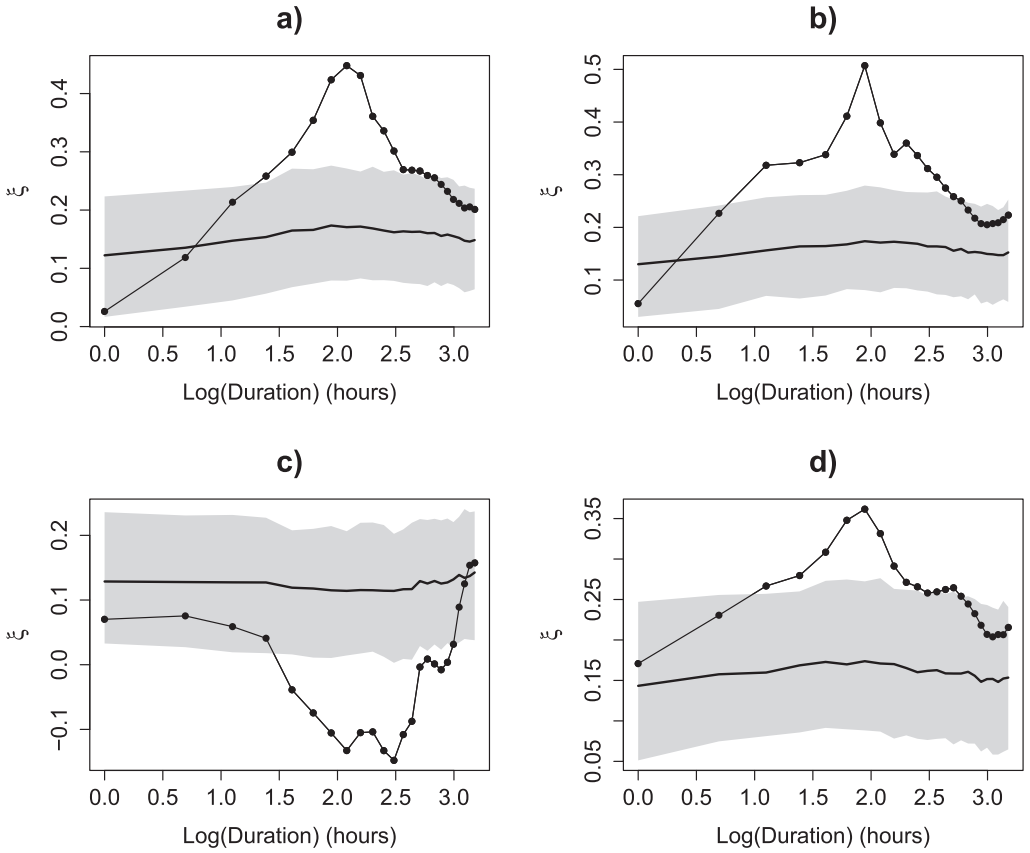

Fig. 5. As in Fig. 3, but for the GEV shape parameter ξ.

employed. The priors for H and θ reflect their conditions of $0 < H \leqslant 1$ and $\theta \geqslant 0$. The prior for H is a Beta distribution nearly flat between 0 and 1, as used in de Vyver (2015, 2018). θ has a flat, non-negative prior with an upper bound at 10. We noticed that the use of other near-flat priors for θ with a larger or infinity upper bound, such as the log-normal distribution used in de Vyver (2015), makes the inference procedure slow and difficult to converge. The prior distribution for $\bar{\xi}$ is relatively flat between 0.3 and -0.15, and is the same as used in Martins and Stedinger (2000) and de Vyver (2015, 2018). The priors for τ_μ^2, τ_σ^2 and τ_ξ^2 are conjugate distributions and typically used in hierarchical Bayesian models (Gelman, 2006; Lunn et al., 2012).

3.1.1. Local estimation of GEV and scaling parameters

Given a set of N rainfall gauges, the question is whether the hyperparameter vector $[H\ \theta\ \alpha\ \beta\ \bar{\xi}\ \tau_\mu^2\ \tau_\sigma^2\ \tau_\xi^2]$ should be (i) individually and independently estimated for each gauge (non-pooled estimators); (ii) estimated considering the entire data set (pooled or regional estimators), or (iii) estimated using an intermediary approach (partial pooled estimators), where the hyperprior distributions of the individual parameters shrink them to some common mean (see, for instance, the eight-school problem in Gelman et al., 2013). In a small watershed or over a homogeneous hydrologic region, it is reasonable to assume that the scaling exponents are similar for the overall rainfall process, indicating that pooled estimators should be preferred.

However, we have observed that the estimation of H, θ, α and β (through Monte Carlo Markov Chain Simulation, see below) is extremely slow and hard to achieve when using pooled or partial pooled estimators. Therefore, for these four hyperparameters, we adopt non-pooled estimators; for the remaining hyperparameters, we adopt pooled (i.e., regional) estimators. If we introduce the subscripts i and j to denote rainfall gauge i and year j, respectively, then using the Bayes theorem (Gelman et al., 2013), we can combine Eqs. (9)–(21) and write the joint posterior distribution of the complete parameter set Θ as:

$$
\begin{aligned}
Pr(\Theta|\mathbf{y}) \propto & \prod_{i=1}^{N}\prod_{j=1}^{T_i}\prod_{d=1}^{24} GEV(y_{d,j,i}|\mu_{d,i},\sigma_{d,i},\xi_{d,i})\cdot \\
& N\left(\log(\mu_{d,i})|\alpha_i - H_i\cdot\log\left(\frac{d+\theta_i}{d_{24}+\theta_i}\right),\ \tau_\mu^2\right)\cdot \\
& N\left(\log(\sigma_{d,i})|\beta_i - H_i\cdot\log\left(\frac{d+\theta_i}{d_{24}+\theta_i}\right),\ \tau_\sigma^2\right)\cdot N(\xi_{d,i}|\bar{\xi},\ \tau_\xi^2)\cdot \\
& N(\alpha_i|0,\ 10^6)\cdot N(\beta_i|0,\ 10^6)\cdot B(H_i|1,\ 1,\ 0,\ 1)\cdot U(\theta_i|0,\ 10)\cdot \\
& B(\bar{\xi}|9,\ 6,\ -0.5,\ 0.5)\cdot Inv\text{-}Gamma(\tau_\mu^2|0.01,\ 0.01)\cdot Inv \\
& -Gamma(\tau_\sigma^2|0.01,\ 0.01)\cdot Inv\text{-}Gamma(\tau_\xi^2|0.01,\ 0.01),
\end{aligned}
\tag{22}
$$

with $\mathbf{y}$ denoting the rainfall intensity data, N the total number of gauges, T_i the total number of years for gauge i, d the duration of rainfall and $d_{24} = 24$. It is worth mentioning that all three GEV parameters will vary across gauges i and durations d, while α, β, H and θ will change only as a function of gauge i, and the remaining parameters are pooled (regional) estimators.

Analytical integration of (22) with respect to the set of parameters Θ is not tractable, and we adopt here the widely used Markov Chain Monte Carlo (MCMC) method to sample from the posterior distribution (22). The model is coded in the R platform and uses the associated packages (Sturtz et al., 2005; Wu et al., 2015) and free software OpenBUGS for the MCMC sampling scheme. The standard code is freely provided as Supplementary material. The simulation considered 20.000 iterations for each of 5 chains. The first 10.000 iterations were discard (burn-in period) and, in order to avoid serial dependence within the MCMC sample, a thinning rate of 50 was used, so that each chain resulted in 200 (10.000/50) samples and the posterior distribution of each parameter had a sample size of 1.000 (200 times 5 chains). The convergence of the posterior distributions was evaluated visually based on the mixture of 5 chains and based on the $\hat{R}$ coefficient, as suggested

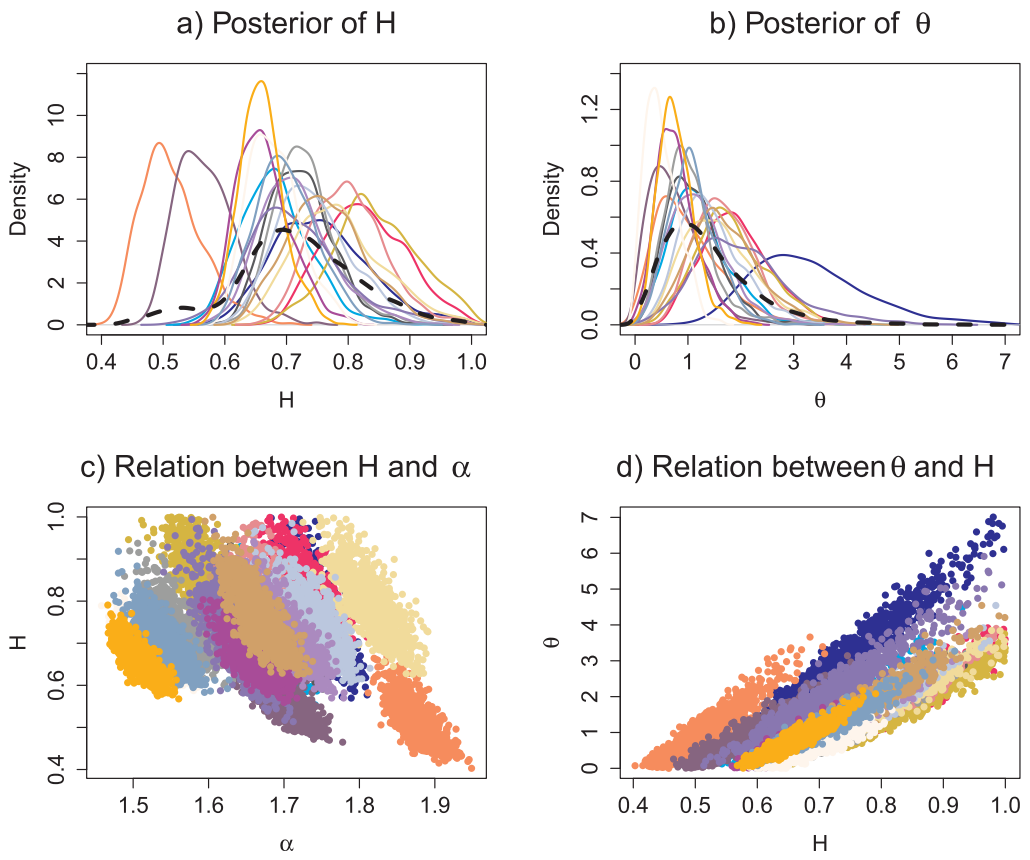

Fig. 6. Bayesian posterior distribution of H, θ, H and α, and θ and H. The different colors represent the 18 gauges used for the Bayesian inference. The dashed lines in (a) and (b) show the posterior distribution resulting from pooling together the simulated values of H and θ estimated at each calibration station to obtain a regional posterior distribution for these parameters.

in Gelman et al. (2013). Convergence was considered achieved when $\hat{R} \leqslant 1.1$, although most values were less than 1.01.

3.1.2. Estimation of GEV parameters for 24-h rainfall for partially gauged sites

For sites that have available only the annual maximum of daily rainfall (partially gauged sites), the procedure previously described cannot be directly used to estimate the GEV parameters for shorter durations, preventing the estimation of IDF curves at the desired scale. In this case, we need first to estimate the equivalent annual maximum rainfall of 24 h duration, which can be accomplished, for instance, using the Hershfield correction factor (e.g., Papalexiou et al., 2016). Then we estimate $\log(\mu_{24}) = \alpha$, $\log(\sigma_{24}) = \beta$ and ξ_{24} in a Bayesian framework. For a given gauge, the joint posterior distribution of μ_{24}, σ_{24} and ξ_{24} is given by:

$$Pr(\mu_{24}, \sigma_{24}, \xi_{24}|\mathbf{y}) \propto \prod_{j=1}^{T} GEV(y_j|\mu_{24}, \sigma_{24}, \xi_{24}) \cdot N(\xi_{24}|\bar{\xi}, \tau_{\xi}^2) \quad (23)$$

with T the number of years for the selected gauge, and y_j the maximum 24-h rainfall for year j. Note that we assume uniform prior distributions for μ_{24} and σ_{24}; for ξ_{24}, we use our prior knowledge and set a prior based on the regional estimates of $\bar{\xi}$ and τ_{ξ}^2 obtained in the previous procedure (Eq. (22)).

The estimation of μ_{24}, σ_{24} and ξ_{24} in (23) for partially gauged sites will follow the same procedure and diagnostic check explained in 3.1.1. Their posterior distributions along with the posterior distributions of H, θ, $\bar{\xi}$, τ_{ξ}^2, τ_{μ}^2, and τ_{σ}^2 previously obtained (from Eq. (22) for gauged sites) will then be used to estimate μ_d, σ_d, and ξ_d, $d = 1, \ldots, 23$, as detailed in Section 4.2. It is worth mentioning that for gauged sites, where rainfall intensity data for all durations are available, μ_{24}, σ_{24} and ξ_{24} are obtained from Eq. (22).

4. Results

4.1. Posterior distributions and scaling of at-site GEV parameters

The relation of the GEV location parameter μ with the rainfall duration is shown in Fig. 3 for four benchmark rainfall gauges (1 = Daegwallyeon; 2 = Suwon; 3 = Yangpyeong; and 4 = Boeun, see location in Fig. 1) randomly selected from the full set of 18 gauges. The 95% credible interval obtained from the posterior distribution is also displayed along with the ordinary GEV estimates, where the parameters are estimated independently for each duration. For the four stations, we clearly observe a nonlinear, monotonic relationship of μ with rainfall duration, supporting our previous assumption as stated in (11). The credible interval includes all point estimates of the ordinary GEV, and its spread increases as duration decreases, reflecting more uncertainty in this range. Results for the remaining rainfall gauges are similar to those observed in Fig. 3 and are not shown here.

Fig. 4 displays the scaling of the GEV scale parameter σ with the rainfall duration for the same benchmark gauges evaluated for μ. A nonlinear relationship is also observed, corroborating our previous assumption as expressed in (12). The spread of the credible intervals is also wider as the duration decreases, reflecting more uncertainty for small durations. However, differently from the credible intervals for μ (Fig. 3), here the intervals do not include all the point estimates from the ordinary GEV. The assumption of scaling and the associated prior distribution for σ (Eq. (12)) tends to produce a smoother curve of σ versus duration than the curve obtained with independent estimates, where no scaling is assumed. This suggests that the prior distribution (i.e. scaling) of σ has a strong power over its posterior distribution (Eq. (22)). When we consider the uncertainty in the ordinary GEV estimates (shown in Supplementary Material), we noticed an overlap of credible and confidence intervals.

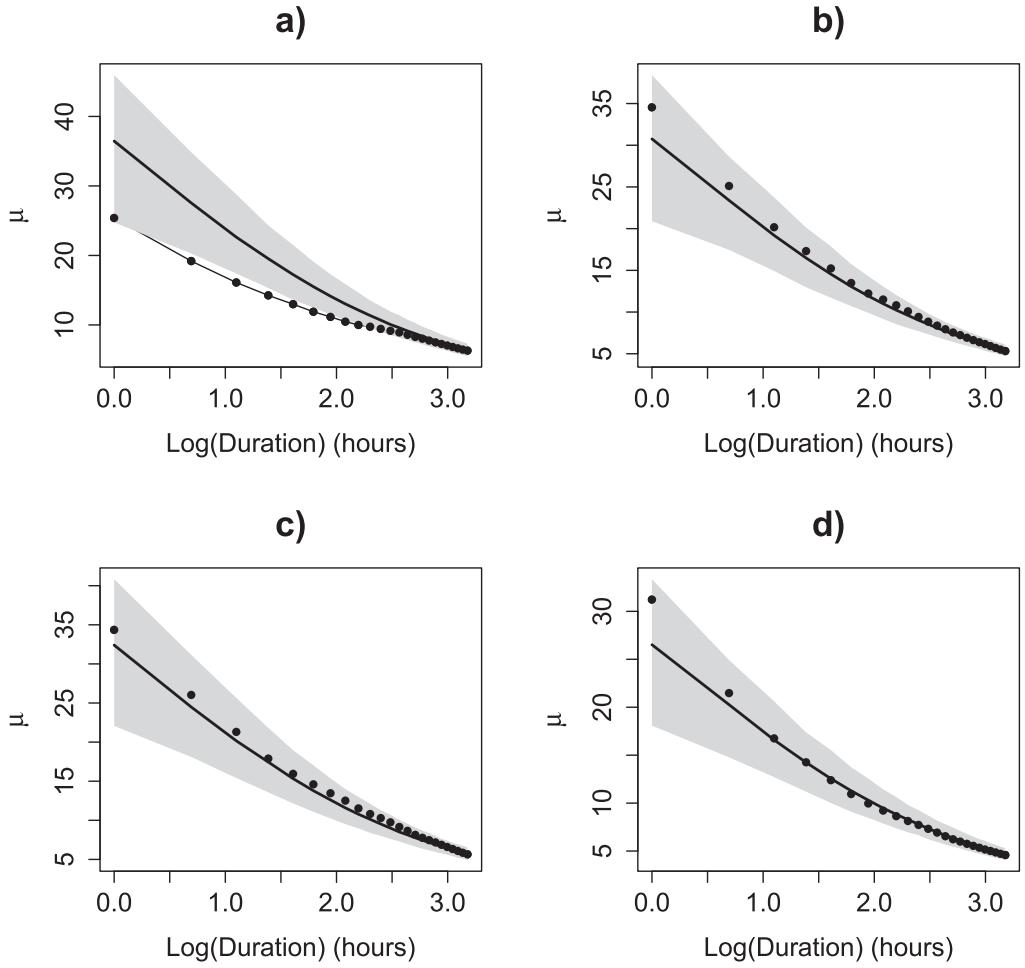

Fig. 7. Scaling of GEV location parameter μ using ordinary GEV (black dots) and the proposed Bayesian model (black line) in a cross-validation scheme for tested gauges (a) Daegwallyeong, (b) Suwon, (c) Yangpyeong, and (d) Boeun. The shaded region shows the 95% credible interval.

The GEV shape parameter ξ does not show any kind of systematic scaling with rainfall duration, as displayed in Fig. 5 and previously assumed in Eq. (13). The traditional GEV estimates for ξ generally fall outside the credible intervals obtained from the Bayesian model, indicating a substantial degree of variability in such estimates. Interestingly, the credible intervals are somehow similar across the four benchmark stations as well as for the other rainfall stations (not shown here), with positive values for most durations, suggesting heavy tailed distributions.

Fig. 6a and b show, respectively, the posterior distributions of H and θ for the entire set of 18 gauges. The dashed lines show the posterior distributions when the individual densities are merged, which can be seen as regional curves. In Fig. 6c, we do not observe any direct relation of H and α (estimation of $\exp(\mu_{24})$), but the spread (i.e. uncertainty) of the posterior distribution of α for a given station is weakly associated with the respective distribution of H. Conversely, H and θ are strongly correlated (Fig. 6d), and it is of utmost importance to consider this relation when simulating these two parameters as input to estimate μ_D, σ_D, and ξ_D for partially gauged sites (see next section). This finding also suggests the possibility to model θ as a function of H directly in the model, which was not explored in this study. As relatively large values of θ appear in the posterior distributions (Fig. 6b), we do not think that it could be omitted as is the case in other studies (e.g., Blanchet et al., 2016) that employed $\theta = 0$.

4.2. Model application I: prediction of GEV parameters for partially gauged sites

The ability of the proposed model to estimate the GEV parameters for partially gauged sites, where rainfalls of short durations are missing but observations of daily rainfall are available, is tested here in a cross-validation scheme, as follows:

1. The rainfall data set for some selected gauges (testing set) are withdrawn from the entire set. Here, the selected gauges are the four benchmark stations previously presented. The remaining gauges (gauged sites) will be used for the inference phase and will be called the calibration set;
2. The posterior distributions of the scaling parameters H and θ as well as of $\bar{\xi}$, τ^2_ξ, τ^2_μ, and τ^2_σ are estimated only for the calibration set of gauges using Eq. (22);
3. The simulated values of H and θ estimated at each calibration station are pooled together to obtain a regional posterior distribution for these parameters (dashed lines in Fig. 6a and b);
4. For each testing gauge (considered now partially gauged sites), the observed 24-h annual maximum rainfall series is used to obtain the posterior distributions of μ_{24}, σ_{24} and ξ_{24} using Eq. (23). The posterior distribution of $\bar{\xi}$ and τ^2_ξ obtained in step 2 is used as the prior

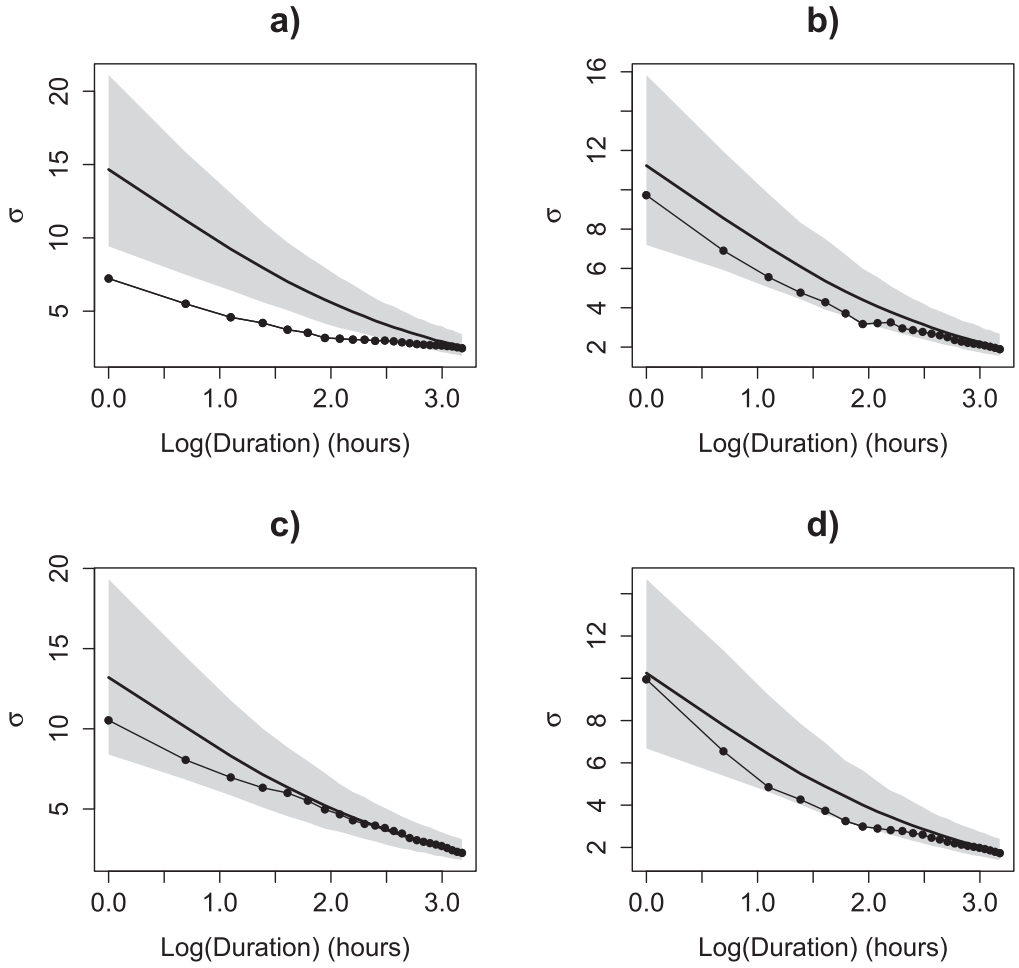

Fig. 8. As in Fig. 7, but for the GEV scale parameter σ.

distribution of ξ. In the case that only annual maximum series of daily rainfall are available, then the Hershfield correction factor (e.g., Blanchet et al., 2016; Papalexiou et al., 2016) should be used to obtain annual maximum series of 24-h duration;

5. For each testing gauge, the posterior distributions of μ_d, σ_d, and ξ_d, where $d = 1, \ldots, 23$ is the rainfall duration, are obtained through the scaling relations expressed in Eqs. (11), (12), and (13) along with the posterior distributions of H, θ, $\bar{\xi}$, τ_ξ^2, τ_μ^2, and τ_σ^2 obtained in step 2. For α and β, we use, respectively, the posterior distributions of $\log(\mu_{24})$ and $\log(\sigma_{24})$ as obtained in step 4.

The scaling of the posterior distributions of μ (step 5) with the rainfall duration for the selected testing gauges is shown in Fig. 7. The 95% credible intervals contain most of the ordinary GEV estimates (obtained using the entire data set, as shown in Fig. 3) and generally follow the pattern obtained from the local Bayesian model (Fig. 3), except that they are wider to account for the larger uncertainties of out-of-sample estimates.

The scaling of the posterior estimates of σ with the rainfall duration for the selected testing gauges is displayed in Fig. 8. With the exception of station # 1 (Daegwallyeon), the wider credible intervals now include most of the ordinary GEV estimates, which was not observed for the local Bayesian model (Fig. 4). For station # 1, the Bayesian estimates for short durations are higher than those from the ordinary GEV model, reflecting more uncertainty. This might be due to the location of the Daegwallyeon site in eastern Korea (Fig. 1), and therefore distant from the major sites, where rainfall data were used to obtain the scaling parameters H and θ.

Finally, the scaling of the posterior estimates of the shape parameter ξ (Fig. 9) is very distinct from those ordinary GEV, but resemble the at-site Bayesian estimates (Fig. 5) using the full data set, with the median estimate being around 0.1. It is worth mentioning here that the model proposed for partially gauged sites imply that ξ has the same posterior distribution across sites and durations, except for sample variations due to the MCMC simulation.

4.3. Model application II: historical Intensity-Duration-Frequency curves for gauged and partially gauged sites

In order to verify how IDF curves produced by the proposed Bayesian model differ from those curves obtained from ordinary GEV, we derive IDF curves based on the median posterior estimates of μ, σ, and ξ simulated by the at-site Bayesian model and as predicted by the Bayesian model for the partially gauged (testing) sites using the scaling-invariant relation (shown in Figs. 7–9). The results are shown in Fig. 10 for the selected rainfall stations # 1 (Daegwallyeon) and # 2 (Suwon). The uncertainty associated with the Bayesian estimates is omitted in these figures to facilitate visualization. Note that the estimates for the partially gauged sites are obtained through a cross-validation scheme, where the rainfall data for the benchmark gauges are withdrawn from the dataset and are not used in the inference process, but they are for the estimation of μ_{24} and σ_{24}.

In general, both Bayesian estimates are very close to the ordinary GEV ones, despite the differences in the distribution parameters as showed in Figs. 3, 4, 7 and 8. The largest differences appear to occur at short durations, where also rainfall intensity (in mm/hr) is higher. In the case of the Daegwallyeon site, the overestimation of the rainfall

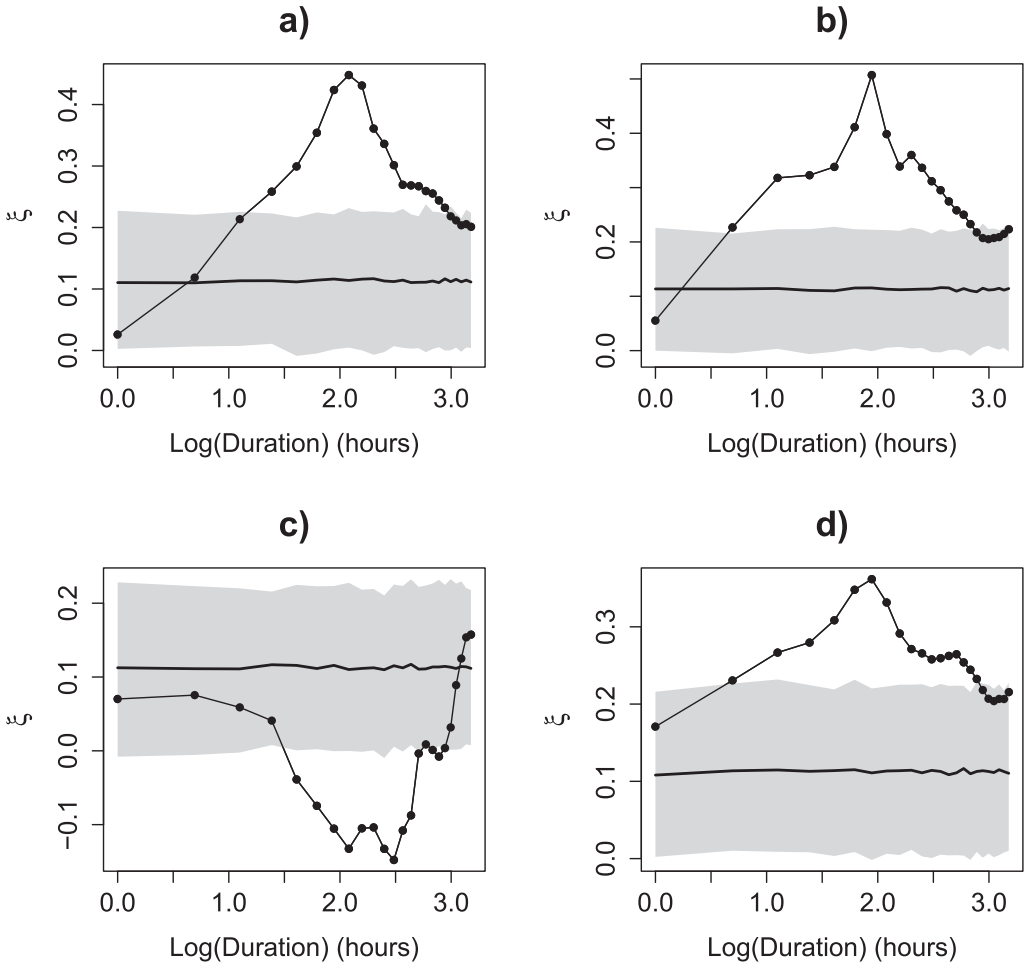

Fig. 9. As in Fig. 7, but for the GEV shape parameter ξ.

intensity obtained in the partially gauged approach is associated with the substantial differences in the GEV parameters (Figs. 7a and 8a). The results for the benchmarks gauges # 3 (Yangpyeong) and # 4 (Boeun) are similar (not shown here).

4.4. Model application III: future climate Intensity-Duration-Frequency curves for gauged sites

The projection of changes in the 24-h annual maximum rainfall (after the bias-correction procedure, as explained in Section 2.2) for the Daegwallyeong station for the period 2011–2100 is displayed in Fig. 11 for RCP scenarios 6 and 8.5. An increase in the frequency of rainfall events of magnitude around 100–200 mm and above 400 mm is projected for both scenarios, while a reduction in the frequency of rainfall of magnitudes 200–300 mm is expected. The main goal of this work is basically to evaluate how these projected changes in 24-h duration annual maximum rainfall will affect IDF curves for local stations but also for the region under study.

The procedure to obtain future IDF curves for gauged sites consists of:

1. The at-site posterior distributions of H, θ and ξ_d obtained using historical data (Section 4.1) as well as the pooled estimates for $\overline{\xi}$, τ_ξ^2, τ_μ^2, and τ_σ^2 are saved;
2. For each site, the projected 24-h annual maximum rainfall series (after bias correction) is used to obtain the posterior distributions of μ_{24} and σ_{24} using the Bayesian model expressed in (23) and the previous simulated values of $\overline{\xi}$ and τ_ξ^2 (step 1) as the prior distribution of ξ;
3. For each site, the predictive posterior distributions of μ_d and σ_d, where $d = 1, \ldots, 24$ is the rainfall duration, is obtained for the future climate through the scaling relations expressed in Eqs. (11) and (12) along with the historical, posterior distributions obtained in step 1. For ξ_d, the historical, posterior distributions of the pooled estimates obtained in step 1 are used in Eq. (13). For α and β, we use, respectively, the future posterior distributions of $\log\mu_{24}$ and $\log\sigma_{24}$ as obtained in step 2.

The IDF curves produced by the at-site Bayesian model for the Daegwallyeong and Suwon stations are shown in Fig. 12. Across scenarios, an increase in the rainfall intensity is expected for scenario RCP 8.5 for the Suwon station, particularly for short durations, while for the Daegwallyeong site a reduction in the intensity is projected for scenario RCP 8.5. When compared with the historical IDF curves produced by the at-site Bayesian model (first column of Fig. 10), we expect a modest increase in the rainfall intensity for both sites and scenarios, notably for short durations.

When the projected changes in future IDF curves are compared with historical IDFs for all sites, we observe, when considering an average estimate across all stations, an increase in the rainfall intensity for all durations and return periods (Fig. 13). The relative difference increases as the return period gets larger, being around 18% for a 100-year return period under scenario RCP 6. It is also interesting to note that, for return periods beyond 25 years, the difference is larger for short durations. The differences projected under scenario RCP 8.5 (Fig. 13b) are larger, being around 25% for a 100-year return period event, but follow similar patterns of those changes projected under scenario RCP 6 (Fig. 13a).

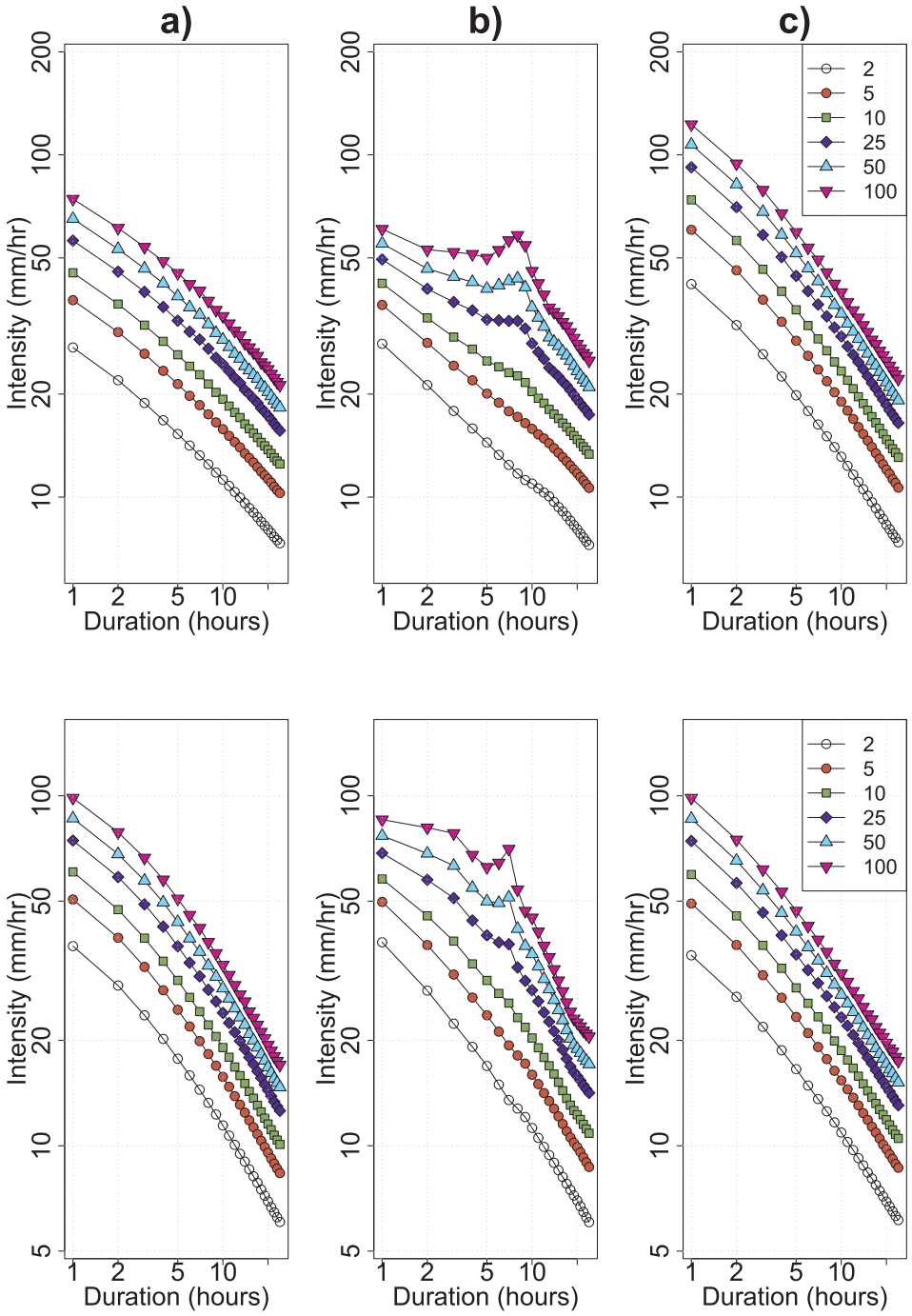

Fig. 10. Historical IDF curves based on the GEV distribution for the benchmark gauges Daegwallyeong (top panels) and Suwon (bottom panels) produced by: (a) the at-site Bayesian model; (b) ordinary GEV; and (c) the Bayesian model considered a partially-gauged site. The legend refers to the return periods 2, 5, 10, 25, 50 and 100 years.

4.5. Model application IV: regional Intensity-Duration-Frequency curves for historical and future climates

In order to minimize noise that can be attributed to downscaled GCM/RCM projections for specific sites, we propose a regional IDF curve using the following procedure:

1. The historical rainfall for all gauged sites is used to estimate the at-site posterior distributions of H and θ and the pooled estimates for $\bar{\xi}$, τ_{ξ}^2, τ_{μ}^2, and τ_{σ}^2 as described before;
2. Using the Bayesian model expressed in (23) and the estimates of $\bar{\xi}$ and τ_{ξ}^2 obtained in step 1, we estimate regional GEV location μ_{24}, scale σ_{24} and shape ξ_{24} parameters for a duration of 24 h after concatenating the observed annual maximum 24-h rainfall for all sites into a single vector;
3. The regional estimates of μ_d, σ_d, and ξ_d, $d = 1, \ldots, 23$, are estimated through the scaling relations expressed in Eqs. (11), (12), and (13) together with the historical, posterior distributions of H, θ, $\bar{\xi}$, τ_{ξ}^2, τ_{μ}^2, and τ_{σ}^2 obtained in step 1. For α and β, we use, respectively, the posterior distributions of $\log\mu_{24}$ and $\log\sigma_{24}$ as obtained in step 2;
4. The regional (historical) IDF curve is obtained using the posterior estimates of μ_d, σ_d, and ξ_d, $d = 1, \ldots, 24$;
5. For future IDF curves, we first apply the bias-correction procedure as previously described to obtain the future projections (scenarios

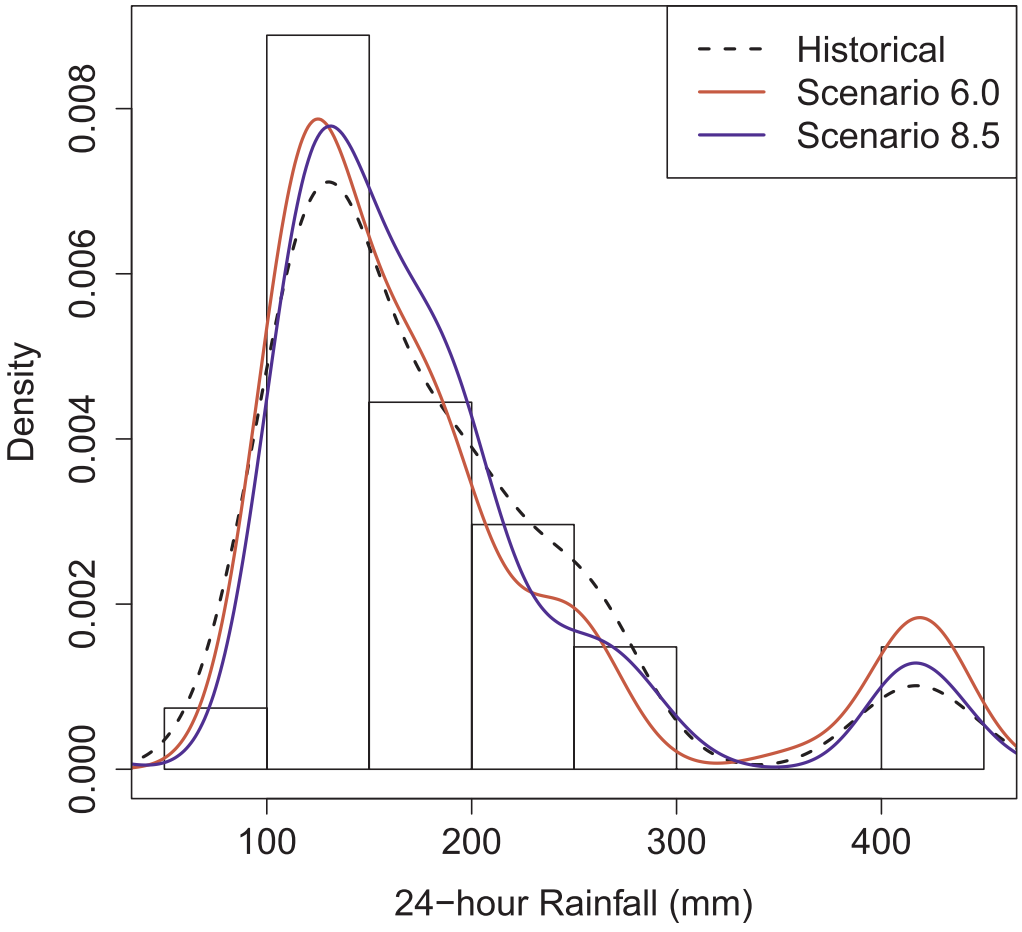

Fig. 11. Histogram and empirical density for the 24-h annual maximum rainfall of observed (dashed line) data for the reference period 1979–2005 and simulated data (red and blue lines) for two different scenarios for the period 2011–2100 and station Daegwallyeong. (For interpretation of the references to colour in this figure caption, the reader is referred to the web version of this article.)

RCP 6 and RCP 8.5) of the annual maximum 24-h rainfall for each site. We then use these projections to estimate the (future) regional GEV parameters μ_{24}, σ_{24} and ξ_{24} as in step 2. The procedures described in steps 3 and 4 are now performed using these estimates to obtain regional future IDF curves for each RCP scenario.

Fig. 14 displays the posterior distributions of μ_{24} and σ_{24} for the historical period and future scenarios RCP 6 and RCP 8.5. A slight shift in the location parameter μ_{24} is observed for both scenarios, but with no apparent differences between their projections. Conversely, a significant increase in the scale parameter σ_{24} is projected for both scenarios, in the order of 30% for RCP 6 and 40% for RCP 8.5. In this sense, the regionally projected changes in rainfall intensity are more associated with changes in variability rather than changes in the mean value.

The historical and future IDF curves obtained for the regional Bayesian model are shown in Fig. 15. For all durations and return periods, we expect an increase in the extreme rainfalls. In terms of relative differences (Fig. 16), the values range from an increase of 7% for a 2-year return period in RCP 6 up to an increase of about 30% for a 100-year return period under scenario RCP 8.5. Such increases now appear larger than those projected when averaging across all stations (Fig. 13) and apparently are more constant along the rainfall duration for a fixed return period.

5. Discussion and summary

A GEV local-regional Bayesian model was proposed to estimate IDF curves based on the scaling-invariant property of the rainfall process. In this context, we estimate sub-daily, at-site GEV parameters for extreme rainfalls as well as for partially and ungauged sites, when using estimates obtained for the 24-h rainfall and the scaling parameters H and θ. The model was applied to rainfall series from 18 stations located in the Han River Watershed in South Korea, to estimate local and regional IDF curves based on the historical record and the future scenarios RCP 6 and RCP 8.5 of daily maximum rainfall generated by the HadGEM2-AO model.

The scaling property of the GEV location and scale parameters with the rainfall duration were confirmed for all sites, considering both ordinary GEV and Bayesian estimates from the proposed model. The shape parameter has no observed scaling, in agreement with the literature (Blanchet et al., 2016). The uncertainty associated with the scaling estimates lead to appreciable differences between ordinary and Bayesian estimates, particularly for short durations. The scaling parameters H and θ are well correlated but we did not observe any significant relation with the location parameter for the 24-h maximum rainfall (α), suggesting that we can merge the at-site posterior distributions of H and θ into a single, regional distribution that can be used to estimate local or regional GEV parameters for short rainfall durations, when only series of annual maximum 24-h rainfall are available. Following this procedure, we obtained GEV estimates for cross-validated, partially gauged sites that satisfactorily agree with the ordinary GEV as well as with those from the proposed local Bayesian model. When compared with ordinary GEV, the Bayesian model proposed here makes use of more information to estimate the parameters as it considers the scaling-invariant property of rainfall in its formulation, leading to a reduction in the associated uncertainty, which can also be easily incorporated in the IDF curves, if desired.

IDF curves derived from the local Bayesian model generally follow the curves obtained from the ordinary GEV model. However, IDF curves obtained for partially gauged sites can overestimate the intensity for short durations and large return periods, and this should be observed when using these curves, particularly for regions where the spatial variability of rainfall is high or the target site is distant from the major

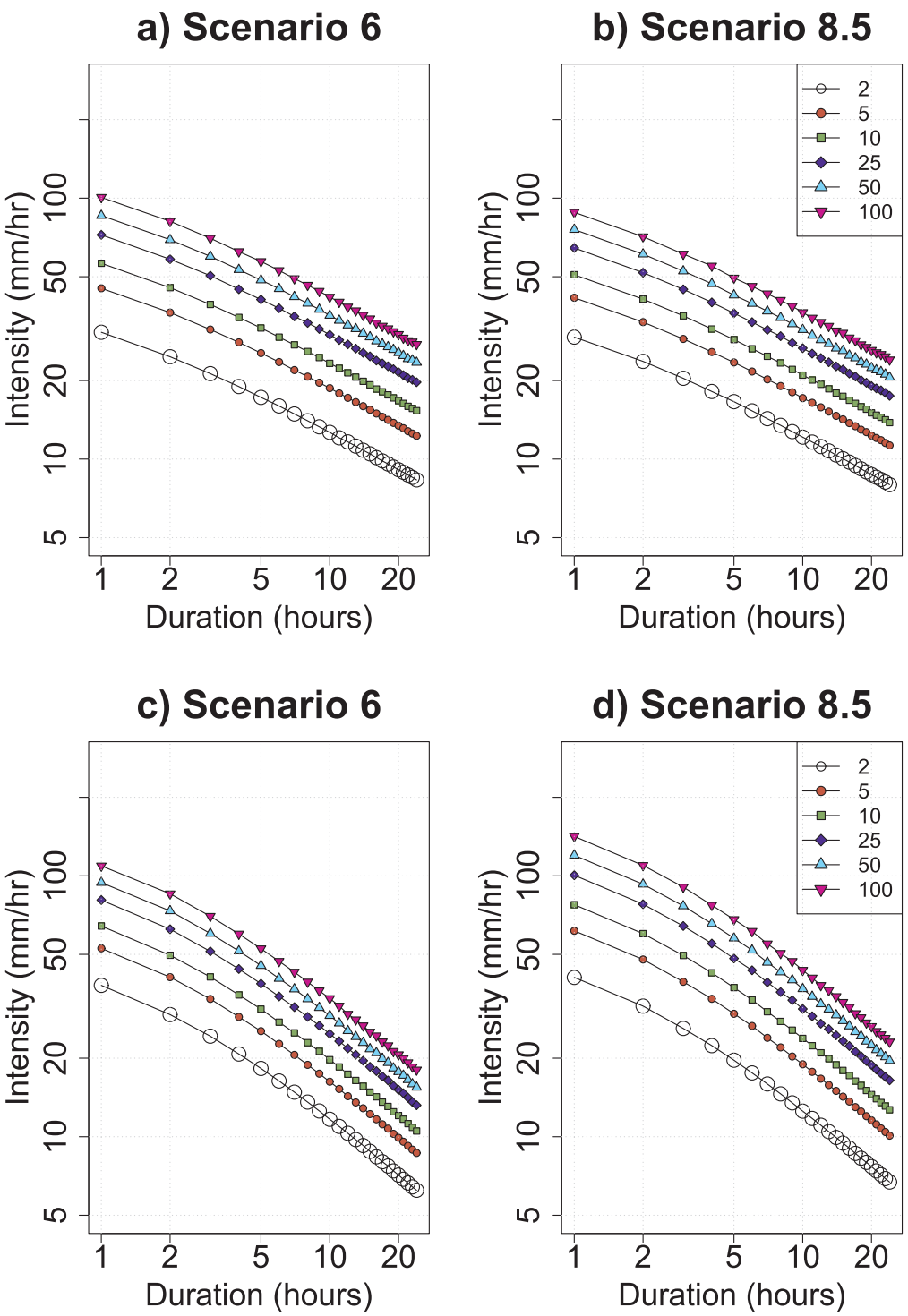

Fig. 12. Future IDF curves for gauges Daegwallyeong (top panels) and Suwon (bottom panels) for scenarios RCP 6 and RCP 8.5 considering the at-site Bayesian model.

ones, whose rainfall data were used to estimate the scaling parameters. Alternatively, in such circumstances we suggest to obtain regional IDF curves using the model proposed in this work and utilize them for partially gauged and ungauged sites. One could also explore the use of at-site estimates of the scaling parameters H and θ to obtain the GEV parameters of short rainfall durations for nearby, partially gauged sites.

When considering future scenarios of rainfall for individual sites, we projected an increase in the rainfall intensity, particularly for rare events (high return periods) and under scenario RCP 8.5. However, local projections might be unreliable due to the high uncertainty in the spatial variability projected by GCMs. In order to address this issue, we proposed a Bayesian model in which regional GEV parameters are estimated for the 24-h maximum rainfall, and the estimates of the scaling parameters are used to estimate regional parameters for shorter durations. Using this approach, we observed that most future changes in rainfall intensity are driven by changes in the scale parameter, i.e., we expect more variability in the extremes. Modest changes in the location are also expected, but there is no difference between their projections from scenarios RCP 6 and RCP 8.5. The projected changes in rainfall intensity are now higher than those obtained when averaging future

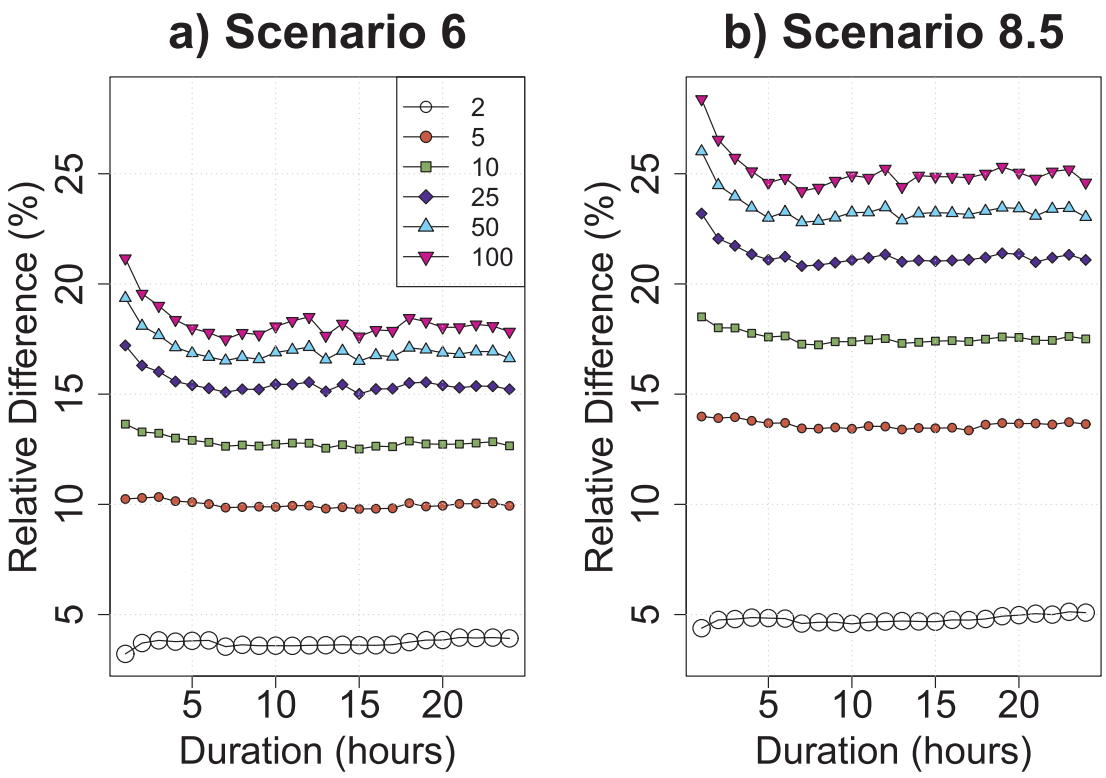

Fig. 13. Average (across stations) relative difference between projected and historical IDF curves. The return periods are indicated in (a).

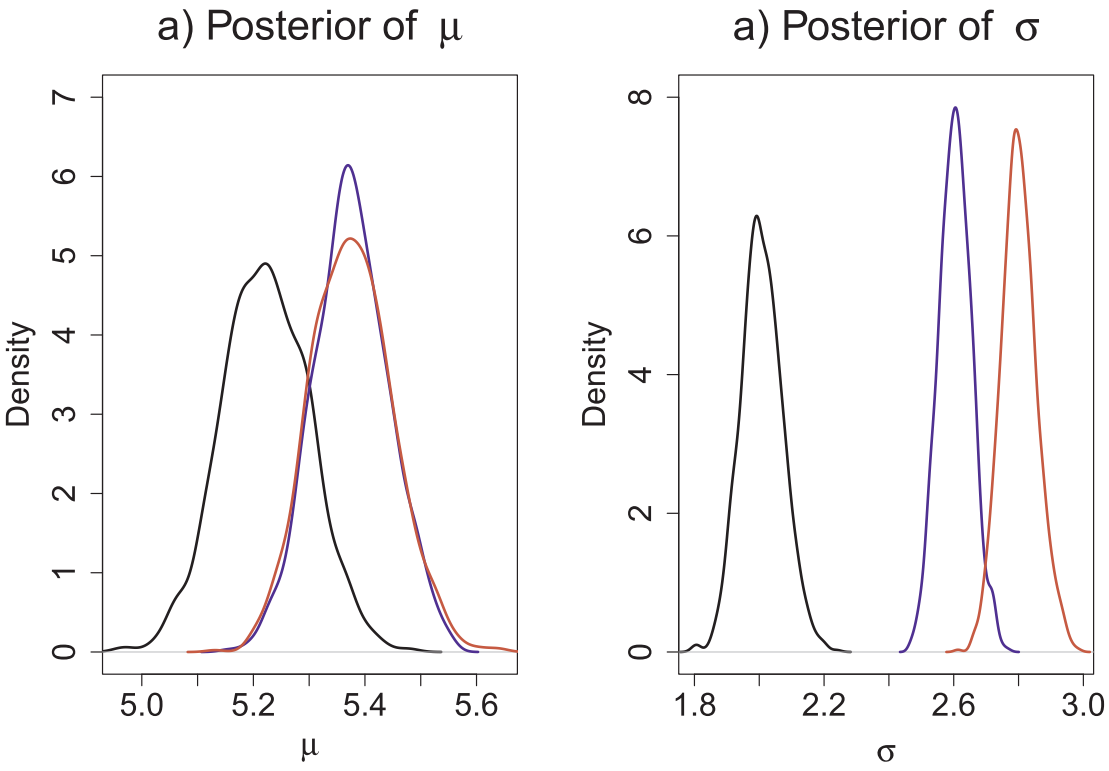

Fig. 14. Regional posterior distribution of location μ_{24} and scale σ_{24} parameters for the historical period (black line) and future scenarios RCP 6 (blue line) and RCP 8.5 (red line). (For interpretation of the references to colour in this figure caption, the reader is referred to the web version of this article.)

estimates across stations. The most pronounced changes (up to about 30% for scenario RCP 8.5) are again expected for rare events (large return periods), but, interestingly, for a fixed return period, the magnitude of changes tends to be constant across durations, contrary to what was obtained for local sites.

To the best of our knowledge, this is the first statistical approach in the literature to estimate future changes in regional IDF curves, which we believe is a more pertinent approach given the high uncertainty in the way GCMs simulated the spatial variability of rainfall. Credible intervals for the expected changes can also be easily incorporated in the

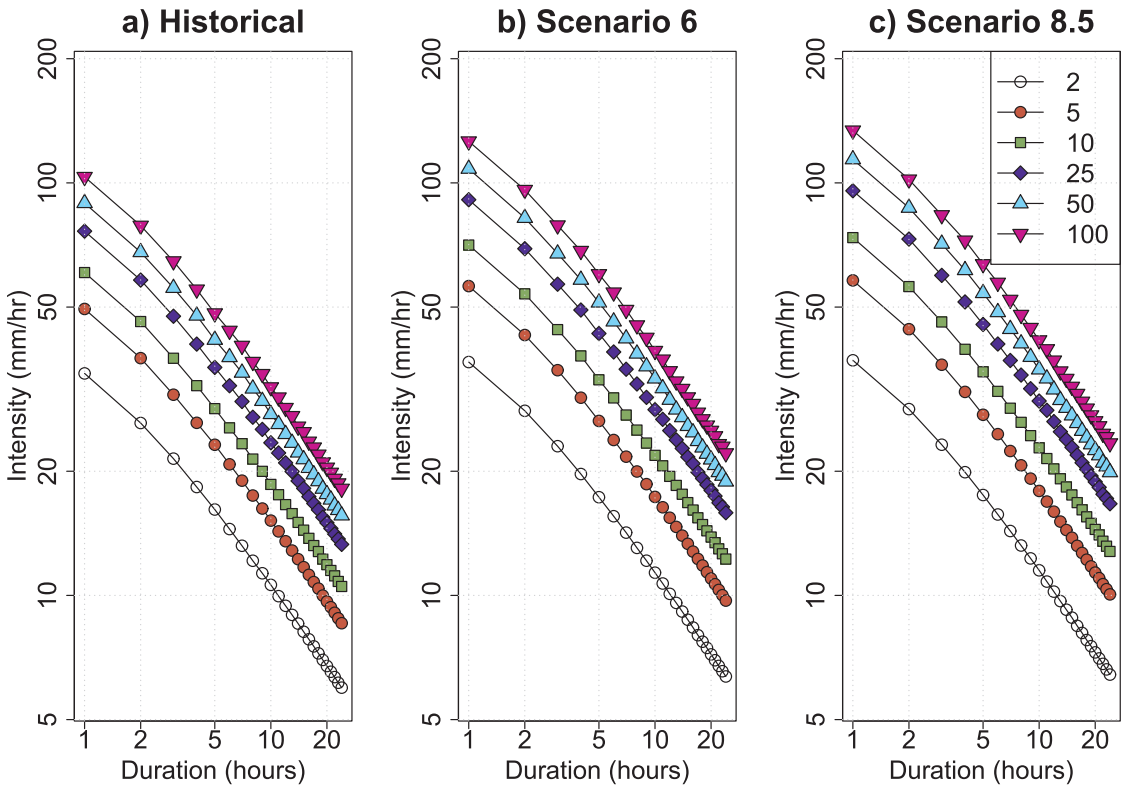

Fig. 15. Regional IDF curves for: (a) historical period; (b) scenario RCP 6; and (c) scenario RCP 8.5.

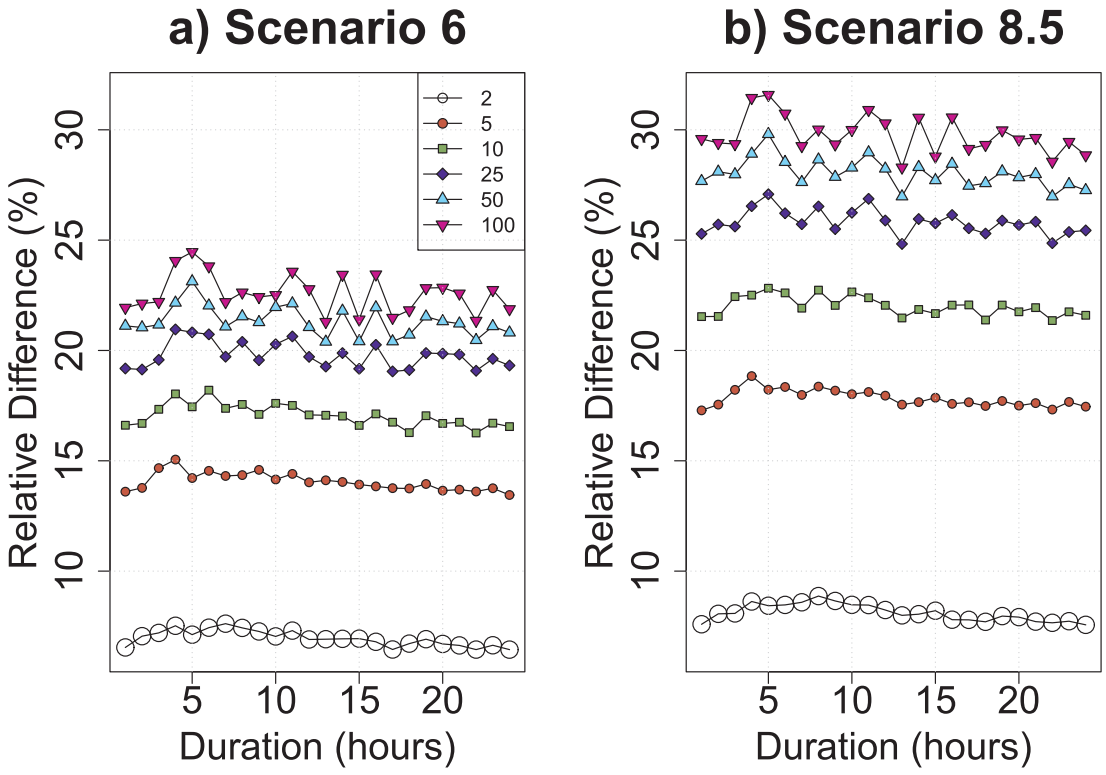

Fig. 16. Relative difference between projected (RCP scenarios 6 and 8.5) and historical regional IDF curves. The return periods are indicated in (a).

regional IDF curves, if requested. We assumed that the scaling pattern of the rainfall process and the posterior distribution of the shape parameter will remain in the future climate as estimated in the historical period. This stationary assumption is crucial for the Bayesian model proposed in this work and it can be hard to evaluate, given the limitations of GCMs to simulate sub-daily rainfall. The results should also be appraised in the context of the HadGEM2-AO model simulations. It is not clear whether such changes will be observed for different GCM simulations. The physical reasons for the expected changes in future IDF curves for the selected rainfall stations were not explored in

this study and will be the theme of future work. A regional model considering larger and more heterogeneous regions will also be explored in future works.

5.1. Acknowledgments

This work was mainly supported by the Korea Agency for Infrastructure Technology Advancement (KAIA) grant funded by the Ministry of Land, Infrastructure and Transport (Grant 18AWMP-B083066-05). This research was partially supported by the MSIT (Ministry of Science and ICT), Korea, under the ITRC (Information Technology Research Center) support program (IITP-2018-2015-0-00378) supervised by the IITP (Institute for Information & Communications Technology Promotion). We also thank Simon Michael Papalexiou and one anonymous Reviewer for the constructive comments that greatly improved the original manuscript.

Appendix A. Supplementary data

Supplementary data associated with this article can be found, in the online version, at https://doi.org/10.1016/j.jhydrol.2018.08.075.

References

Baek, H.-J., Lee, J., Lee, H.-S., Hyun, Y.-K., Cho, C., Kwon, W.-T., Marzin, C., Gan, S.-Y., Kim, M.-J., Choi, D.-H., Lee, J., Lee, J., Boo, K.-O., Kang, H.-S., Byun, Y.-H., 2013. Climate change in the 21st century simulated by HadGEM2-AO under representative concentration pathways. Asia-Pac. J. Atmos. Sci. 49 (5), 603–618. https://doi.org/10.1007/s13143-013-0053-7.

Berg, N., Hall, A., 2015. Increased interannual precipitation extremes over california under climate change. J. Clim. 28, 6324–6334.

Blanchet, J., Ceresetti, D., Molinié, G., Creutin, J.-D., 2016. A regional GEV scale-invariant framework for Intensity–Duration–Frequency analysis. J. Hydrol. 540 (Supplement C), 82–95. URL http://www.sciencedirect.com/science/article/pii/S0022169416303584.

Chow, V.T., Maidment, D.R., Mays, L.W., 1988. Applied Hydrology. McGraw-Hill.

Coles, S., 2001. An Introducton to Statistical Modeling of Extreme Values. Springer.

Davies, T., Cullen, M.J.P., Malcolm, A.J., Mawson, M.H., Staniforth, A., White, A.A., Wood, N., 2005. A new dynamical core for the Met Office's global and regional modelling of the atmosphere. Q.J.R. Meteorolog. Soc. 131 (608), 1759–1782. https://doi.org/10.1256/qj.04.101.

de Vyver, H.V., 2015. Bayesian estimation of rainfall intensity-duration-frequency relationships. J. Hydrol. 529, 1451–1463. URL http://www.sciencedirect.com/science/article/pii/S0022169415006083.

de Vyver, H.V., 2018. A multiscaling-based intensity-duration-frequency model for extreme precipitation. Hydrol. Processes 32 (11), 1635–1647.

Gaume, E., Gaál, L., Viglione, A., Szolgay, J., Kohnová, S., Blöschl, S., 2010. Bayesian MCMC approach to regional flood frequency analyses involving extraordinary flood events at ungauged sites. J. Hydrol. 394 (1–2), 101–117. URL http://linkinghub.elsevier.com/retrieve/pii/S0022169410000193.

Gelman, A., 2006. Prior distributions for variance parameters in hierarchical models. Bayesian Anal. 1 (3), 515–533.

Gelman, A., Carlin, J.B., Stern, H.S., Dunson, D.B., Vehtari, A., Rubin, D.B., 2013. Bayesian Data Analysis, third ed. CRC Press.

Ghanmi, H., Bargaoui, Z., Mallet, C., 2016. Estimation of intensity-duration-frequency relationships according to the property of scale invariance and regionalization analysis in a Mediterranean coastal area. J. Hydrol. 541 (Part A), 38–49. URL http://www.sciencedirect.com/science/article/pii/S0022169416304322.

Grimaldi, S., Kao, S.-C., Castellarin, A., Papalexiou, S.-M., Viglione, A., Laio, F., Aksoy, H., Gedikli, A., 2011. 2.18 – Statistical Hydrology. In: Wilderer, P. (Ed.), Treatise on Water Science. Elsevier, Oxford, pp. 479–517. URL https://www.sciencedirect.com/science/article/pii/B9780444531995000464.

Gudmundsson, L., Bremnes, J.B., Haugen, J.E., Engen-Skaugen, T., 2012. Downscaling RCM precipitation to the station scale using statistical transformations – a comparison of methods. Hydrol. Earth Syst. Sci. 16, 3383–3390.

Gyasi-Agyei, Y., 2005. Stochastic disaggregation of daily rainfall into one-hour time scale. J. Hydrol. 309 (1), 178–190. URL http://www.sciencedirect.com/science/article/pii/S0022169404005712.

Haddad, K., Rahman, A., Stedinger, J.R., 2012. Regional flood frequency analysis using Bayesian generalized least squares: a comparison between quantile and parameter regression techniques. Hydrol. Processes 26 (7), 1008–1021. URL http://doi.wiley.com/10.1002/hyp.8189.

Hosseinzadehtalaei, P., Tabari, H., Willems, P., 2018. Precipitation intensity-duration-frequency curves for central Belgium with an ensemble of EURO-CORDEX simulations, and associated uncertainties. Atmos. Res. 200, 1–12.

Koutsoyiannis, D., 1994. A stochastic disaggregation method for design storm and flood synthesis. J. Hydrol. 156 (1), 193–225. URL http://www.sciencedirect.com/science/article/pii/0022169494900787.

Koutsoyiannis, D., Kozonis, D., Manetas, A., 1998a. A mathematical framework for studying rainfall intensity-duration-frequency relationships. J. Hydrol. 206 (1), 118–135. URL http://www.sciencedirect.com/science/article/pii/S0022169498000973.

Koutsoyiannis, D., Kozonis, D., Manetas, A., 1998b. A mathematical framework for studying rainfall intensity-duration-frequency relationships. J. Hydrol. 206 (1), 118–135. URL http://www.sciencedirect.com/science/article/pii/S0022169498000973.

Kwon, H.-H., Brown, C., Lall, U., 2008. Climate informed flood frequency analysis and prediction in Montana using hierarhical Bayesian modeling. Geophys. Res. Lett. 35, 1–6.

Li, J., Johnson, F., Evans, J., Sharma, A., 2017. A comparison of methods to estimate future sub-daily design rainfall. Adv. Water Resour. 110, 215–227. URL http://www.sciencedirect.com/science/article/pii/S0309170817301422.

Liang, Z., Chang, W., Li, B., 2011. Bayesian flood frequency analysis in the light of model and parameter uncertainties. Stochastic Environ. Res. Risk Assess. 26 (5), 721–730. URL http://link.springer.com/10.1007/s00477-011-0552-y.

Lima, C.H., Kwon, H.-H., Kim, J.-Y., 2016. A Bayesian beta distribution model for estimating rainfall IDF curves in a changing climate. J. Hydrol. 540 (Supplement C), 744–756. URL http://www.sciencedirect.com/science/article/pii/S0022169416304243.

Lima, C.H.R., Lall, U., 2010. Spatial scaling in a changing climate: a hierarchical Bayesian model for non-stationary multi-site annual maximum and monthly streamflow. J. Hydrol. 383, 307–318.

Lunn, D., Jackson, C., Best, N., Thomas, A., Spiegelhalter, D., 2012. The BUGS Book: A Practical Introduction to Bayesian Analysis. Chapman and Hall/CRC.

Martins, E.S., Stedinger, J.R., 2000. Generalized maximum-likelihood generalized extreme-value quantile estimators for hydrologic data. Water Resour. Res. 3 (3), 737–744.

Mélèse, V., Blanchet, J., Molinié, G., 2018. Uncertainty estimation of Intensity-Duration-Frequency relationships: a regional analysis. J. Hydrol. 558, 579–591. URL http://www.sciencedirect.com/science/article/pii/S002216941730519X.

Menabde, M., Seed, A., Pegram, G., 1999. A simple scaling model for extreme rainfall. Water Resour. Res. 35 (1), 335–339. https://doi.org/10.1029/1998WR900012.

Muller, A., Bacro, J.-N., Lang, M., Jan 2008. Bayesian comparison of different rainfall depth–duration–frequency relationships. Stochastic Environ. Res. Risk Assess. 22 (1), 33–46. https://doi.org/10.1007/s00477-006-0095-9.

Nguyen, V.T.V., Nguyen, T.D., Wang, H., 1998. Regional estimation of short duration rainfall extremes. Water Sci. Technol. 37 (11), 15–19. URL http://wst.iwaponline.com/content/37/11/15.

Papalexiou, S.M., Dialynas, Y.G., Grimaldi, S., 2016. Hershfield factor revisited: correcting annual maximum precipitation. J. Hydrol. 542, 884–895. URL http://www.sciencedirect.com/science/article/pii/S0022169416306254.

Ragno, E., AghaKouchak, A., Love, C.A., Cheng, L., Vahedifard, F., Lima, C.H.R., 2018. Quantifying changes in future intensity-duration-frequency curves using multimodel ensemble simulations. Water Resour. Res., n/a–n/a. https://doi.org/10.1002/2017WR021975.

Renard, B., 2011. A Bayesian hierarchical approach to regional frequency analysis. Water Resour. Res. 47 (11), n/a–n/a. URL http://doi.wiley.com/10.1029/2010WR010089.

Renard, B., Lang, M., Bois, P., 2006. Statistical analysis of extreme events in a non-stationary context via a Bayesian framework: case study with peak-over-threshold data. Stochastic Environ. Res. Risk Assess. 21 (2), 97–112. URL http://link.springer.com/10.1007/s00477-006-0047-4.

Ringer, M.A., Martin, G.M., Greeves, C.Z., Hinton, T.J., James, P.M., Pope, V.D., Scaife, A.A., Stratton, R.A., Inness, P.M., Slingo, J.M., Yang, G.-Y., 2006. The physical properties of the atmosphere in the new hadley centre global environmental model (hadgem1). Part II: aspects of variability and regional climate. J. Clim. 19, 1302–1326.

Segond, M.-L., Onof, C., Wheater, H., 2006. Spatial–temporal disaggregation of daily rainfall from a generalized linear model. J. Hydrol. 331 (3), 674–689. URL http://www.sciencedirect.com/science/article/pii/S0022169406003258.

Singh, V.P., 1992. Elementary Hydrology. Prentice-Hall.

Sivakumar, B., Sorooshian, S., Gupta, H.V., Gao, X., 2001. A chaotic approach to rainfall disaggregation. Water Resour. Res. 37 (1), 61–72. https://doi.org/10.1029/2000WR900196.

So, B.-J., Kim, J.-Y., Kwon, H.-H., Lima, C.H., 2017. Stochastic extreme downscaling model for an assessment of changes in rainfall intensity-duration-frequency curves over South Korea using multiple regional climate models. J. Hydrol. 553, 321–337. URL http://www.sciencedirect.com/science/article/pii/S0022169417305255.

Sturtz, S., Ligges, U., Gelman, A., 2005. R2WinBUGS: a package for running WinBUGS from R. J. Stat. Software 12 (3), 1–16. URL http://www.jstatsoft.org.

van Montfort, M.A., 1990. Sliding maxima. J. Hydrol. 118 (1), 77–85. URL http://www.sciencedirect.com/science/article/pii/002216949090251R.

Viglione, A., Merz, R., Salinas, J.L., Blöschl, G., 2013. Flood frequency hydrology: 3. A Bayesian analysis. Water Resour. Res. 49 (2), 675–692. URL http://doi.wiley.com/10.1029/2011WR010782.

Wu, H., Godfrey, A.J.R., Govindaraju, K., Pirikahu, S., 2015. ExtDist: extending the range of functions for probability distributions. R package version 0.6-3. URL http://CRAN.R-project.org/package=ExtDist.

Yu, P.-S., Yang, T.-C., Lin, C.-S., 2004. Regional rainfall intensity formulas based on scaling property of rainfall. J. Hydrol. 295 (1), 108–123. URL http://www.sciencedirect.com/science/article/pii/S0022169404001362.

Zhang, W., Villarini, G., Nov 2017. Heavy precipitation is highly sensitive to the magnitude of future warming. Clim. Change 145 (1), 249–257. https://doi.org/10.1007/s10584-017-2079-9.